


## Effect of surfactant in an airway closure model

F. Romanò <sup>\*</sup>

*Univ. Lille, CNRS, ONERA, Arts et Métiers Institute of Technology, Centrale Lille, UMR 9014, LMFL  
(Laboratoire de Mécanique des Fluides de Lille), Kampé de Fériet, F-59000 Lille, France*

M. Muradoglu

*Department of Mechanical Engineering, Koç University, Istanbul 34450, Turkey*

J. B. Grotberg

*Department of Biomedical Engineering, University of Michigan, Ann Arbor, Michigan 48109, USA*



(Received 27 April 2022; accepted 7 September 2022; published 21 September 2022)

A model of the bronchioles lined by the airway surface liquid is employed to investigate the Plateau-Rayleigh instability that can lead to the occlusion of the airways. This physiologically relevant phenomenon is normally occurring in distal airways, i.e., in the bronchioles from the seventh generation on. Special attention is paid to the effect of surfactant dispersed in the liquid phase and along the liquid-gas interface. A single-layer Newtonian film is simulated in a rigid capillary pipe in order to isolate the impact of the surfactant and unravel their complex dynamics coupled with the multiphase liquid-gas dynamics. Apart from the primary instability leading to airway closure, we focus on the postcoalescence wall stresses and stress gradients produced by the bifrontal plug growth. With our model, we demonstrate that increasing the surfactant concentration and their strength, the airway closure slows and the wall stresses are reduced up to 20%. Within the physiological application intended for our model, we study the stability of the multiphase system. We predict the generation at which airway closure will occur depending on the liquid lining thickness and the initial surfactant concentration.

DOI: [10.1103/PhysRevFluids.7.093103](https://doi.org/10.1103/PhysRevFluids.7.093103)

### I. INTRODUCTION

Among the several domains one could consider in biological and medical sciences, pulmonology is one the most fruitful in terms of variety of fundamental problems inspiring the fluid mechanics community. At the same time, fundamental studies in respiratory fluid mechanics often provided a guide through the physiological complexity of the problem, highlighting leading-order effects that drive undesired phenomena correlated to widespread pathologies. This is the case, for instance, of the occlusion and reopening of the airways, usually termed airway closure and airway reopening, respectively, and both explained due to classical fluid mechanics arguments.

In fact, the annular liquid coating the bronchioles gives rise to a multiphase flow in a deformable capillary pipe. For the first 15 or 16 airway generations, the multiphase flow involves three phases, i.e., air, mucus, and serous or periciliary liquid [1], while the problem becomes a two-phase system (air and a waterish fluid) from the 16th or 17th generation on. In healthy patients, the one- and two-liquid layers lining the inner wall of the airways are relatively thin, ranging from 2% to 4% of the airway radius. However, when pathological conditions lead to hypersecretion of mucus, the relative

---

<sup>\*</sup>francesco.romano@ensam.eu

film thickness can increase up to 40% of the airway radius [2], exceeding the critical threshold after which an infinitesimal perturbation of the air-mucus interface leads to the formation of a liquid plug within a breathing cycle [3]. The resulting airway closure can drive the collapse of the corresponding bronchioles [4,5] and block the air exchange at distal airways. Such a well-documented medical problem has inspired several fluid mechanics models that helped understanding the underlying physical mechanism. The surface tension at the air-mucus interface, responsible of interfacial capillary forces, drives an axial pressure gradient that drains fluid from the thin film coating the airway walls and brings it to the interface bulge until a liquid plug is formed. Such a phenomenon, known as Plateau-Rayleigh instability [6,7], results from the interfacial pressure jump directly proportional to the surface tension and to the air-mucus interface cross-sectional curvature. These fundamental fluid mechanics problems explain why thicker liquid films are more prone to induce airway closure, as the gas-liquid interface possesses a higher cross-sectional curvature [8]. Moreover, as the instability is driven by surface tension, surfactant replacement therapies are commonly employed to control the Plateau-Rayleigh instability by reducing the average surface tension in order to limit the occurrence of airway closure events.

Owing to the predictive achievements of theoretical approaches, increasingly refined models have been proposed to study airway closure from first principles. Some of them focused on the onset of the Plateau-Rayleigh instability, relying on a leading-order approximation of the continuity and Navier-Stokes equations valid for thin films. This is the case of [9], who investigated the fluid-elastic instabilities for an airway closure model in deformable capillary pipes, or of [10], who included the effect of surfactant in order to predict how increasing their concentration changes the onset of the capillary instability. Along the same wit, Ref. [11] focused on the effect of viscoelasticity on the pre-coalescence phases of distal airway closure. All these studies reliably predict the onset of the instability and, making use of the lubrication theory, they unravelled a number of physiologically interesting effects due to the extension they considered to the canonical Plateau-Rayleigh liquid-lined capillary pipe model, including two-layer lining [12].

As such models rely on the asymptotic thin film approximation, they cannot be used to predict airway closure phases shortly before coalescence and after the liquid plug has been formed. In fact, when the instability-driven interface bulge grows, the thin film asymptotic limit breaks down and more general models must be employed. To investigate such a dynamics, one should rather consider the full Navier-Stokes equation and eventually solve it numerically. This approach has been used by [13], who simulated the whole pre-coalescence process demonstrating that complex three-dimensionalities can arise due to the coupling between the cross-sectional mechanical instabilities of the bronchioles walls and the capillary instabilities of the lining liquid. They showed that the fluid-structure interaction leads to a quicker and fully three-dimensional airway closure. Other models rather focused on the wall stresses and stress gradients produced by a Newtonian airway closure during the pre-coalescence [14] process, showing that they are compatible with a lethal or sublethal response of the epithelium [15–17]. Only recently, the whole closure process has been numerically simulated. By including both, pre- and postcoalescence phases [8], discovered that the so-called bifrontal plug growth leads to postcoalescence stresses that can be 300% to 600% higher than pre-coalescence values. This is in agreement with corresponding experimental results [18,19], and it has been confirmed also by [12], who generalized the model to a two-layer coating and found that the airway closure can occur in much shorter times than what predicted by single-layer models. All these studies confirm the potential of airway closure in damaging the epithelial cells on the bronchioles wall, and a recent paper of [20] discovered that a viscoelastic instability arising after closure can lead to comparable stress levels for repeated elastic oscillation events triggered by the bifrontal plug growth for high elastic numbers. Along the same line, corresponding studies have been carried out for the airway reopening, investigating the effect of surfactant [21,22], non-Newtonian effects [23,24], and compliance of airway walls [25]. For dedicated reviews, we refer the reader to [26–29].

In this paper we investigate the effect of surfactant on a Newtonian airway closure in an axisymmetric model, including pre- and postcoalescence. Numerical simulations are carried out for

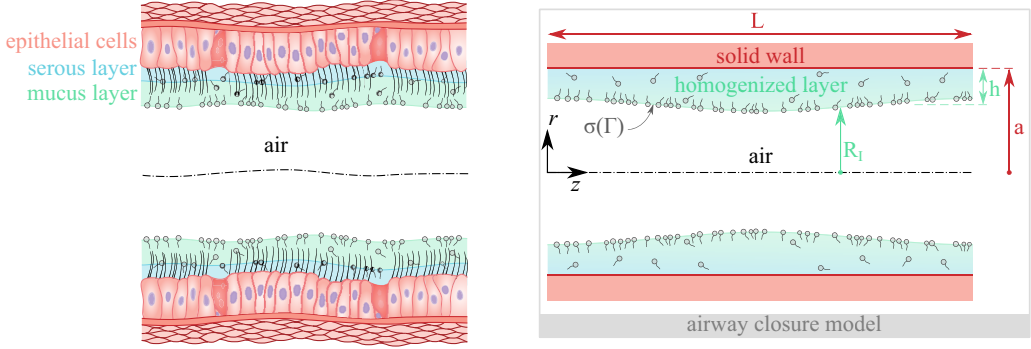


FIG. 1. Schematic of the human airway (left) and the airway model: the ciliated epithelium (left) is simplified to a rigid tube of radius  $a$  and length  $L$  (light red, right), the coating two-layer non-Newtonian liquid (light blue and light green, left) is modeled by a homogenized layer of average total thickness  $h$  (gradient color, right), and the presence of surfactant (gray) is included in both systems.  $R_1(z)$  denotes the radial location of the liquid-gas interface in the airway model.

biologically relevant parameters, also relevant to surfactant replacement therapies. The rest of the paper is organized as follows. The problem formulation is presented in Sec. II. Section III deals with the numerical method employed to discretize the mathematical model; Sec. IV presents the results discussing the effect of the surfactant parameters and the stability properties of the system in light of its physiological interpretation. Finally, Sec. V summarizes the paper and draws the conclusions of our study.

## II. PROBLEM FORMULATION

We consider an airway closure model aimed at investigating the sole effect of the surfactant in the liquid phase. Within our model framework, fluid-structure interactions and complex rheological properties are neglected, and the two-liquid-layer coating the airway wall is homogenized into a single-layer liquid. To this end, the ciliated epithelium is simplified considering a cylindrical rigid tube of radius  $a$  and length  $L$ . Airway closure is therefore studied lining the wall with a Newtonian liquid film of dynamic viscosity  $\mu_L$ , density  $\rho_L$ , and initial average film thickness  $h$ . The innermost phase is the gas core of constant dynamic viscosity  $\mu_G$  and density  $\rho_G$ . The surface tension between the liquid and the gas phase is assumed to depend on the interfacial concentration of surfactant (see Fig. 1).

The airway closure is triggered perturbing the interface location by an initial first-Fourier-mode varicose perturbation

$$r = R_1(t = 0) = a - h[1 - A \times \cos(2\pi z/L)], \quad (1)$$

where  $z$  and  $r$  denote the axial and radial coordinates, respectively,  $t$  is the time,  $A$  is the amplitude of the perturbation and  $R_1$  is the interface location. Nondimensionalizing the length, time, pressure, and velocity by  $a$ ,  $\mu_L a / \sigma_0$ ,  $\sigma_0 / a$ ,  $\sigma_0 / \mu_L$ , respectively, where  $\sigma_0$  is the reference surface tension (initial average surface tension), the multiphase flow encompassing the gas and liquid phases is governed by the one-field equations [30]

$$\vec{\nabla} \cdot \vec{u} = 0, \quad (2a)$$

$$\text{La} \left[ \frac{\partial(\tilde{\rho}\vec{u})}{\partial t} + \vec{\nabla} \cdot (\tilde{\rho}\vec{u}\vec{u}) \right] = -\vec{\nabla} p + \vec{\nabla} \cdot [\tilde{\mu}(\vec{\nabla}\vec{u} + \vec{\nabla}^T\vec{u})] + \int_A [\sigma(\Gamma)\kappa\vec{n} + \vec{\nabla}_s\sigma(\Gamma)]\delta(\vec{x} - \vec{x}_f)dA, \quad (2b)$$

where the continuity equation for incompressible flows is defined by (2a), while (2b) is the momentum equation. The spatial and temporal coordinates are denoted by  $\vec{x}$  and  $t$ ,  $\vec{u}$  and  $p$  are the velocity and pressure fields, respectively, and  $\Gamma$  is the interfacial surfactant concentration normalized with the maximum equilibrium concentration  $\Gamma_\infty$ . In the integral,  $\kappa$  is twice the mean curvature,  $\vec{n}$  a unit vector normal to the interface,  $A$  is the surface area,  $\delta$  the three-dimensional Dirac delta function,  $\vec{x}_f$  denotes the points at the interface,  $\vec{\nabla}_s$  is the interface gradient operator along the interface,  $\vec{\nabla}_s = \vec{\nabla} - \vec{n}(\vec{n} \cdot \vec{\nabla})$ , and  $\sigma$  is the surface tension normalized with respect to  $\sigma_0$  and it is assumed to decrease upon an increase of  $\Gamma$ . Following [31] and [32], it yields

$$\sigma = \begin{cases} (1 - \beta\Gamma) & \text{if } \Gamma < 1, \\ (1 - \beta) \exp\left[\frac{\beta(1-\Gamma)}{1-\beta}\right] & \text{if } \Gamma \geq 1. \end{cases} \quad (3)$$

As discussed by [31] and [32], the surface tension  $\sigma$  varies linearly (at leading order) with the interfacial surfactant concentration  $\Gamma$  for  $\Gamma < 1$ . On the other hand,  $\sigma$  becomes a nonlinear function of  $\Gamma$  for  $\Gamma \geq 1$ . In the nonlinear regime, the surface tension asymptotically approaches a constant minimum value when the interfacial surfactant concentration reaches the maximum packing value. References [31] and [32] assumed an exponential decay of  $\sigma$  for  $\Gamma \geq 1$  and thus obtained the present equation of state that well approximates the pulmonary surfactant monolayer. This same equation of state has been also used by other researchers in similar contexts (see, e.g., [21,33]) and it is demonstrated to be a reliable constitutive equation for dilute surfactant concentrations  $\Gamma$ , as the ones considered in this study.

The normal-stress jump due to surface tension and the Marangoni stress at the interface,  $\vec{\nabla}_s \sigma(\Gamma)$ , are included by means of the integral, typical of the one-field formulation. Moreover, in the one-field formulation, the physical properties of the multiphase fluid are discontinuously defined over the domain. This is the case of the density and the dynamic viscosity fields,  $\tilde{\rho} = \phi + \rho(1 - \phi)$  and  $\tilde{\mu} = \phi + \mu(1 - \phi)$ , respectively, defined via the indicator function  $\phi$  that equals zero in the gas phase and one in the liquid.

Four nondimensional groups are identified in (2), which together with the geometric nondimensional parameters, define the following six dimensionless numbers:

$$\text{La} = \frac{\sigma_0 \rho_L a}{\mu_L^2}, \quad \varrho = \frac{\rho_G}{\rho_L}, \quad \mu = \frac{\mu_G}{\mu_L}, \quad \beta = \frac{\mathcal{R}T\Gamma_\infty}{\sigma_0}, \quad \lambda = \frac{L}{a}, \quad \varepsilon = \frac{h}{a}, \quad (4)$$

where  $\text{La}$  is the Laplace number,  $\varrho$  and  $\mu$  are the density and dynamic viscosity ratios, respectively,  $\beta$  is the elasticity number,  $\mathcal{R}$  is the ideal gas constant,  $T$  is the absolute temperature,  $\lambda$  is the length-to-radius aspect ratio, and  $\varepsilon$  is the average nondimensional film thickness.

Since the normalized surface tension  $\sigma$  is function of  $\Gamma$ , the following constitutive model for surfactant transport is introduced to complement (2). Scaling the bulk surfactant concentration with the critical micelle concentration  $C_{\text{cmc}}$ ,

$$\frac{1}{A} \frac{D(\Gamma A)}{Dt} = \frac{1}{\text{Sc}_s \text{La}} \nabla_s^2 \Gamma + \dot{S}_\Gamma, \quad (5a)$$

$$\frac{\partial C}{\partial t} + \vec{\nabla} \cdot (C\vec{u}) = \frac{1}{\text{ScLa}} \vec{\nabla} \cdot (\tilde{D}\vec{\nabla}C) + \dot{S}_C, \quad (5b)$$

where (5a) is the equation derived by [34] to describe the dynamics of interfacial surfactant, and (5b) models the nondimensional bulk surfactant concentration  $C$  by an advection-diffusion equation with a source term, the material derivative is defined as  $D_t = \partial_t + \vec{u} \cdot \vec{\nabla}$ , and the molecular diffusion field for the surfactant in the bulk  $\tilde{D} = \phi$  since the molecular diffusion is neglected in the gas phase. The bulk and interfacial surfactant concentration dynamics are coupled by the source terms  $\dot{S}_C$  and  $\dot{S}_\Gamma$  that describe the transfer of surfactant from the bulk to the surface and vice versa by taking into account the macroscopic adsorption, desorption, and saturation phenomena for surfactant at the

interface. The  $\dot{S}_\Gamma$  is modeled as in [21]:

$$\dot{S}_\Gamma = \begin{cases} \frac{K_a}{\text{LaSc}_s} C_s(1 - \Gamma) - \frac{K_d}{\text{LaSc}_s} \Gamma & \text{if } \Gamma < 1, \\ -\frac{K_d}{\text{LaSc}_s} \Gamma & \text{if } \Gamma \geq 1, \end{cases} \quad (6)$$

where  $C_s$  is the surfactant concentration in the liquid phase at contact with the interface. The source term in the bulk,  $\dot{S}_C$ , is dealt with making use of the adsorption layer concept developed in [35], hence by assuming that the transfer of the surfactant mass between the interface and the bulk takes place in a thin layer near the interface. We refer the reader to [35] for more details about the implementation of the bulk and surface source terms, as well as about the detailed interpretation of the adsorption layer.

Five new nondimensional groups arise due to (5)

$$\text{Sc} = \frac{\mu_L}{\rho_L D_L}, \quad \text{Sc}_s = \frac{\mu_L}{\rho_L D_S}, \quad K_a = \frac{k_a C_{\text{cmc}} a^2}{D_S}, \quad K_d = \frac{k_d a^2}{D_S}, \quad \chi = \frac{\Gamma_\infty}{C_{\text{cmc}} a}, \quad (7)$$

where  $\text{Sc}$  is the bulk Schmidt number,  $\text{Sc}_s$  the interfacial Schmidt number,  $K_a$  and  $K_d$  are the nondimensional adsorption and desorption coefficients,  $\chi$  is the penetration depth (derived from the redistribution of surfactant mass in the adsorption layer),  $D_S$  and  $D_L$  are the molecular diffusion coefficients on the interface and in the bulk (in liquid phase), respectively, and  $k_a$  and  $k_d$  are the adsorption and the desorption coefficients. Finally, we also assume that the material properties remain constant following the fluid trajectory

$$\frac{D\tilde{q}}{Dt} = 0, \quad \frac{D\tilde{\mu}}{Dt} = 0, \quad \frac{D\tilde{D}}{Dt} = 0. \quad (8)$$

### III. NUMERICAL METHOD

The finite-difference/front-tracking (FD/FT) method of [35,36] is used to discretize the continuity and Navier-Stokes equations (2) fully coupled with the evolution model for the bulk and interfacial surfactant concentration (5). The projection method of [37,38] is applied to a staggered Eulerian grid for discretizing the bulk equations (2) and (5b), and preserving the coupling between them. The numerical scheme is second-order accurate in space for all the terms of the system except for the convective term of the advection-diffusion equation (5b), for which we use the fifth-order WENO-Z scheme of [39]. Owing to the small time step requirements for preserving the numerical stability of the discrete problem, the time derivatives are discretized by a first-order accurate scheme. This approach is found to minimize the computational cost, keeping the share of the temporal error negligible with respect to the spatial one.

In combination with the steady Eulerian grid, a Lagrangian grid consisting of marker points and in-between front elements is simply advected in the domain by the local flow velocity computed on the Eulerian grid. The marker points and the front elements of the Lagrangian grid are used to track the liquid-gas interface and to solve the interfacial surfactant concentration equation (5a). The same spatial and temporal accuracy is used for (5a) as for the bulk equations discretized on the Eulerian grid. Unlike the Eulerian grid, the Lagrangian grid is reconstructed at every time step either adding or removing front elements and markers. This is necessary to prevent a too dense or a too coarse discrete front, and to deal with topological changes of the interface. The reader is referred to [30] for detailed information about the Lagrangian grid reconstruction, and to [21,40] for a sensitivity analysis on the numerical parameters used when topological changes of Lagrangian grid are implemented in our front-tracking method for airway reopening problems. Special attention is paid to maintain strict mass conservation of the interfacial surfactant concentration  $\Gamma$  when reconstructing the Lagrangian grid. For more details about the mass-conservative algorithm in use in this study, we refer to [35].

The synergistic use of Eulerian and Lagrangian approaches is not only limited to the advection of the front. In fact, after tracking the interface, the indicator function  $\phi$  is reconstructed on the Eulerian grid at each time step based on the location of the Lagrangian front (see [41]). Such indicator function is used to set the fluid properties  $\tilde{\rho}$ ,  $\tilde{\mu}$ , and  $\tilde{D}$ , to compute the bulk surfactant concentration in the immediate proximity of the liquid–gas interface  $C_s$ , and to distribute the source term  $\dot{S}_C$  following the adsorption layer model of [35]. Finally, the computation of the surface tension is carried out on the Lagrangian grid and then transferred to the Eulerian staggered grid points by means of Peskin’s cosine distribution functions [42], which are included in (2b) by using a body-force approach [41].

The FD/FT code used in this study has been extensively tested for airway closure and airway reopening problems including surfactant and topological changes of the interface. The most recent comparisons of our code with other numerical solvers and experimental results are reported in [8,20,21] for parameters relevant to our investigation. Such studies demonstrate the satisfactory accuracy of our FD/FT code, hence we refer the reader to them rather than further validating our solver.

#### IV. RESULTS AND DISCUSSION

The liquid plug formation in adult human lungs is the investigation framework of our study, with a special focus on the effect of surfactant throughout the whole process. Since we are interested in surface-tension dominated flows, where airway closure is physiologically relevant, we limit our study to small bronchioles for which gravitational effects can safely be neglected [as assumed by (2b)]. Hence, to characterize a regime for which gravitational forces are negligible, we consider the static Bond number  $\text{Bo}$ :

$$\text{Bo} = \frac{ga^2(\rho_L - \rho_G)}{\sigma_0}, \quad (9)$$

where  $g$  is the gravitational acceleration.

For the first 14 lung generations the power-law fit of [43] holds,  $a_n = a_0 2^{-n/3}$ , where  $a_0 \in [0.75, 1]$  cm is the radius at the zeroth generation (trachea) and  $a_n$  is the radius at the  $n$ th generation (see, e.g., [44]). Considering that, for healthy conditions, the mucus-to-air mean surface tension is  $\sigma_0 \approx 20$  dyn cm<sup>-1</sup>, and for pathological conditions  $\sigma_0 \approx 50$  dyn cm<sup>-1</sup> [45], and assuming  $\rho_L \approx 1$  g cm<sup>-3</sup> and  $\rho_G \approx 10^{-3}$  g cm<sup>-3</sup>, the static bond number as function of the lung generations is depicted in Fig. 2. Based on this order-of-magnitude estimate, for individuals with surfactant deficiency and a small trachea ( $a_0 = 0.75$  cm and  $\sigma_0 \approx 50$  dyn cm<sup>-1</sup>), the gravitational effects can be neglected already starting from generation 8. On the other hand, for healthy patients with a large trachea ( $a_0 = 1$  cm and  $\sigma_0 \approx 20$  dyn cm<sup>-1</sup>), gravitational effects are negligible only from the 11th generation on. Healthy patients with small trachea and pathological cases with large trachea lie in between, i.e., the tenth and ninth generation, respectively.

Based on this characterization of the small-Bond-number regime ( $\text{Bo} < 0.3$ ), we conclude that the range of the mucus-to-air Laplace number of interest for our model should consider airways from the eighth generation on for small tracheas ( $a < 0.12$  cm) if the patient suffers of surfactant deficiency ( $\sigma_0 \approx 50$  dyn cm<sup>-1</sup>) and from the tenth generation on for small tracheas ( $a < 0.07$  cm) if the patient is healthy ( $\sigma_0 \approx 20$  dyn cm<sup>-1</sup>). This latter case leads to higher Laplace numbers. Considering that the dynamic viscosity of mucus may vary over several orders of magnitudes, ranging from 10 to 10 000 times larger than that of water, i.e.,  $\mu_M \in [0.1, 100]$  poise, the Laplace number is  $\text{La} \lesssim 350$ . We will then consider a baseline case with  $\text{La} = 100$  and slightly enlarge the range of admissible Laplace numbers to make sure that all the physiologically relevant  $\text{La}$  are taken into account,  $\text{La} = [50, 500]$ . Following [8,20], the length-to-radius ratio of the airway is set equal to  $\lambda = 6$ , while the nondimensional film thickness is considered to vary within the range  $\varepsilon \in [0.125, 0.3]$ , which includes biologically relevant values. These values of normalized thickness for the airway surface liquid (terminus technicus in the corresponding physiology literature) exceed



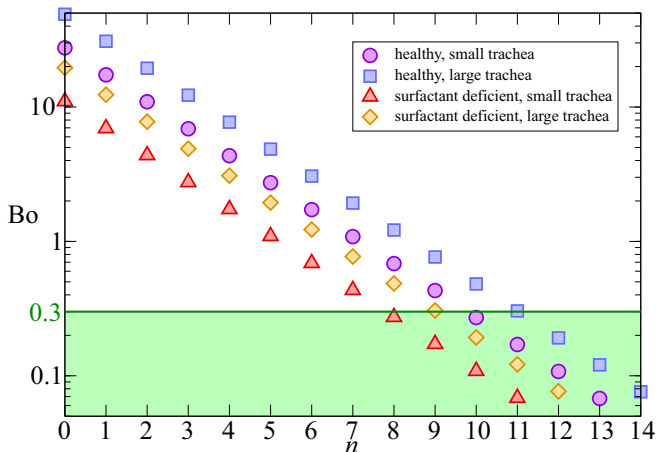


FIG. 2. Order-of-magnitude estimate of the static Bond number as function of the lung generation. The green area denotes the working framework of our investigation for which gravitational effects are safely neglected ( $Bo < 0.3$ ).

the  $\varepsilon$  for regular healthy conditions ( $\varepsilon \approx 0.05$ ). The range of  $\varepsilon$  selected in our study rather applies to the airway mucus accumulation extensively reported by physiologists as a result of the conversion of water-secreting serous cells into mucus secreting cells induced by asthma, chronic bronchitis, cystic fibrosis, and other inflammatory lung diseases [46]. Moreover, we set  $A = 10\%$  as in [8,20]. The choice of this amplitude is made considering that the mechanism at the core of the airway closure is the Plateau-Rayleigh instability, which is a linear instability. This means that the interface perturbation grows exponentially until it is small enough. Hence, only large-enough initial perturbations are of physiological relevance as they lead to airway closures that develop in a time shorter than a typical breathing cycle. The expected critical mode is  $2\pi \approx \lambda = 6$ , hence the most dangerous mode (1) is still dominant over the others. We stress, however, that nonlinear effects due to nonmodal initial conditions could impact the capillary drainage of coating films and collars (see [47]), but they are out of the scope of this study.

For pulmonary surfactant, the critical micelle bulk concentration is  $C_{cmc} \approx 10^{-3}$  g/cm<sup>3</sup> and the adsorption and desorption kinetics are  $k_a \approx 1.7 \times 10^3$  cm<sup>3</sup>/g s and  $k_d \approx 1.7 \times 10^{-2}$  1/s [48,49]. According to the measurements of [50], the surface diffusivity of pulmonary surfactant is  $D_s \in [10^{-7}, 7 \times 10^{-7}]$  cm<sup>2</sup>/s, which leads to baseline values of the nondimensional absorption and desorption coefficients of  $K_a = 10^4$  and  $K_d = 10^2$ , respectively. In our study, we will carry out a sensitivity analysis for these two parameters within the ranges  $K_a \in [10^3, 10^5]$  and  $K_d \in [10, 10^3]$ , as done in [21]. Following the estimate of [51], the maximum equilibrium interfacial concentration for pulmonary surfactant is  $\Gamma_\infty \approx 3.1 \times 10^{-7}$  g/cm<sup>2</sup>, hence the baseline value of the dimensionless adsorption depth is assumed to be  $\chi \approx 0.01$ . The importance of  $\chi$  will, however, be tested within the range  $\chi \in [0.001, 1]$ . Finally, following [31], the baseline Schmidt numbers are set to  $Sc_s = 100$  and  $Sc = 10$ , and following [48], the baseline value of the elasticity number is set to  $\beta = 0.7$ . A sensitivity analysis to such parameters choice will be carried out considering the ranges  $Sc_s \in [10, 100]$  and  $Sc \in [1, 10]$ , as done in [21].

#### A. Analysis of surfactant effects in a typical airway closure scenario

A typical airway closure scenario is here presented by simulating our model for the baseline parameters,  $La = 100$ ,  $C_0 = 10^{-4}$ ,  $\beta = 0.7$ ,  $Sc = 10$ ,  $Sc_s = 100$ ,  $K_a = 10^4$ ,  $K_d = 10^2$ ,  $\chi = 0.01$ , and  $\varepsilon = 0.25$ . Figure 3 depicts the dynamics of the liquid-lined system initially perturbed by a varicose perturbation of 10% of amplitude. The Plateau-Rayleigh instability develops naturally in

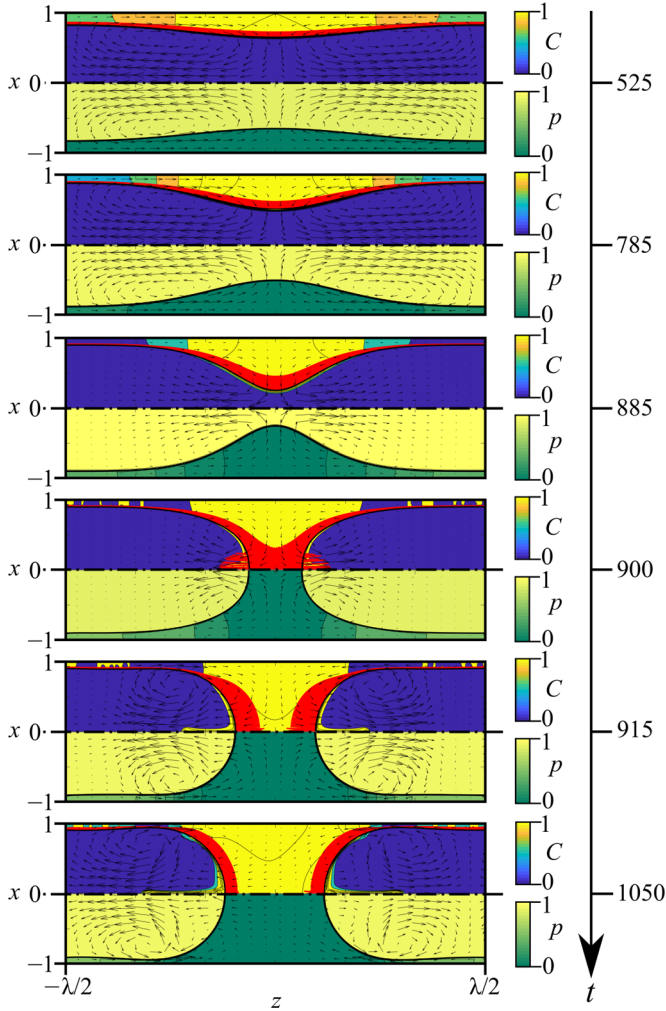


FIG. 3. Airway closure for  $La = 100$ ,  $C_0 = 10^{-4}$ ,  $\beta = 0.7$ ,  $Sc = 10$ ,  $Sc_s = 100$ ,  $K_a = 10^4$ ,  $K_d = 10^2$ ,  $\chi = 0.01$ , and  $\varepsilon = 0.25$ . Top panels: Surfactant concentration in the bulk  $C$  normalized with  $C_0$ ,  $\tilde{C}$ . The surfactant concentration at the interface  $\Gamma$  is depicted by red segments normal to the interface whose length is proportional to  $\Gamma$ . Bottom panels: pressure field. The arrows denote the flow velocity, and the thick black line depicts the interface.

such a configuration, draining liquid from the thin film at the wall and driving it towards the bulge where the pressure has its minimum (see bottom panel at  $t = 525$  in Fig. 3). This is due to the surface tension at the liquid-gas interface that reduces the pressure proportionally to the local cross section curvature of the interface ( $R_1^{-1}$ ). The more the fluid gets drained from the thin film and transported to the bulge, the more the pressure at the bulge decreases with respect to the thin-film pressure, the faster the draining, the faster the bulge grows. On the other hand, for thinner liquid film at the wall it becomes increasingly difficult to drain liquid. As a result, if the initial liquid lining the airway wall is thick enough, the surface tension destabilization overcomes the increasing draining resistance of the thin film and the Plateau-Rayleigh instability leads to the formation of a liquid plug (occurring between  $t = 885$  and  $t = 900$  in Fig. 3), and to a successive bifrontal plug growth responsible of a significant increase of stresses at the airway wall [8]. It is expected therefore that an increase of the surface tension (hence of the Laplace number  $La$ ) will further destabilize the



interface driving a quicker airway closure. On the other hand, a thinner initial film thickness ( $\varepsilon$ ) would rather tend to oppose the closure of the airway, slowing it down or even preventing it by leading to the thin film pinch-off.

Such a well-understood dynamics has been extensively reported in literature, and it holds for Newtonian single- and double-layer coating, as well as for viscoelastic airway closure [8,12,14,18,20]. In this paper, we aim at investigating the effects of surfactant that locally reduce the surface tension and create Marangoni stresses, i.e., interfacial stresses that drive the flow along the interface from low to high surface tension regions. The top panels in Fig. 3 report the scalar field of surfactant concentration in the bulk  $C$  normalized with  $C_0$ ,  $\bar{C}$ , together with the interfacial surfactant concentration  $\Gamma$  depicted in red. In the initial phases of the liquid plug formation, the  $\Gamma$  remains almost uniformly distributed along the interface, leading to an effective reduction of the average surface tension  $\sigma_0$ , hence of the average Laplace number (average of the local Laplace number based on the local surface tension). Marangoni stresses are of minor importance during the early precoalescence phase (see  $t = 525$  in Fig. 3). The draining of liquid from the thin film to the bulge tends, however, to transport the surfactant towards the center of the capillary pipe leading to an increase of the surface tension gradient, hence of the Marangoni stress. As the surface tension at the bulge is lower than that at the thin film, the corresponding solutocapillary effect tends to oppose the airway closure pulling the interface from low-surface-tension (bulge) towards high-surface-tension regions (thin film). The combined effect of the surfactant distributed on the interface is therefore a twofold net stabilizing effect for the Plateau-Rayleigh instability: (1) the reduction of the average Laplace number limits the impact of the capillary instability, and (2) the Marangoni stresses along the interface tend to redistribute the liquid from the bulge towards the thin film. It is therefore expected that increasing the initial concentration of surfactant will slow down the airway closure (see the following sections for a quantitative analysis).

The postcoalescence phase is interpreted along the same line. In fact, the strong interfacial concentration of surfactant initially distributed at the interface of the two retracting air fingers leads to two simultaneous effects. On the one hand, the local reduction of surface tension slows down the recovery of a spherical-cap shape of the interface. On the other hand, the Marangoni stress drives fluid from the liquid plug to the thin film, playing in favor of an ellipsoidal interfacial geometry (see  $t = 900$  and  $t = 915$  in Fig. 3). The further draining leading to the bifrontal plug growth tends, however, to recover the equilibrium condition for the interface, leading to a quasispherical shape for the trailing fronts of the two retracting air fingers in the airway closure model.

Such a nontrivial dynamics will be further investigated in the following sections, with a special focus on the stress and stress gradients at the airway wall, owing to their physiological significance for the bronchioles epithelium.

### B. Effect of the initial bulk surfactant concentration $C_0$ and elasticity number $\beta$

The effect of bulk surfactant concentration is investigated carrying out a parametric study on the initial bulk concentration  $C_0 \in [10^{-5}, 5 \times 10^{-4}]$ , and keeping all the other model parameters fixed, for  $La = 100$ ,  $\beta = 0.7$ ,  $Sc = 10$ ,  $Sc_s = 100$ ,  $K_a = 10^4$ ,  $K_d = 10^2$ ,  $\chi = 0.01$ , and  $\varepsilon = 0.25$ . The relevance of this parametric study is motivated either by pathological conditions corresponding to a surfactant deficiency or by surfactant replacement therapies commonly in use as medical treatments to favor airway reopening and inhibit successive liquid plug formation.

Upon an increase of the bulk surfactant concentration  $C_0$ , the average surface tension decays nonuniformly all along the liquid-gas interface and leads to a net decrease of the average local Laplace number  $\bar{La} = \langle La\sigma/\sigma_0 \rangle < La$ , as well as to a redistribution of Marangoni stresses induced by the surface tension gradients. For the considered parameters, the reduction of average capillary stresses dominates over the impact of Marangoni stresses, that are (of minor) relevance only for the liquid plug dynamics immediately prior to and after closure. As a result, Fig. 4 demonstrates that increasing  $C_0$  slows down the Plateau-Rayleigh instability leading to a longer closure time  $t_c$ . We remark, however, that the relative increment of the closure time is strongly nonlinear. In fact, for

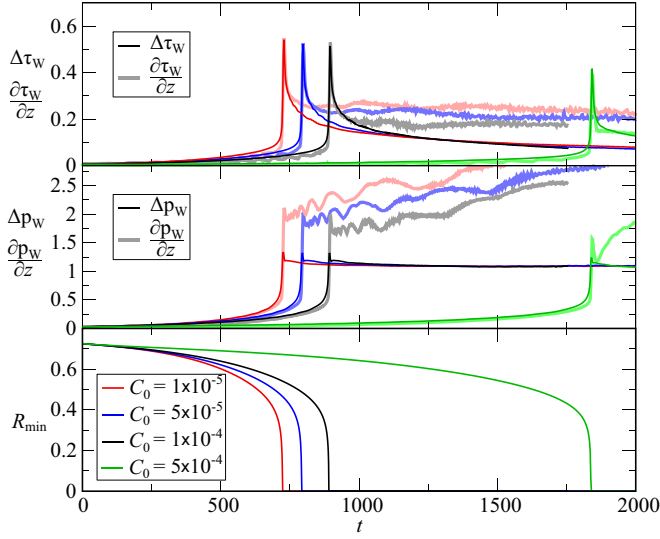


FIG. 4. Effect of the bulk surfactant concentration. Bottom: minimum of the radial location of the interface,  $R_l$  (solid line). Middle: excursion of the normal stress distribution along the wall,  $\Delta p_w(t) = \max_z p(r=1) - \min_z p(r=1)$  (light-colored bold line), and the maximum axial wall pressure gradient  $\max |\partial_z p(r=1)|$  (dark-colored line). Top: excursion of the tangential stress distribution along the wall,  $\Delta \tau_w(t) = \max_z \tau(r=1) - \min_z \tau(r=1)$  (light-colored bold line), and the maximum axial wall shear stress gradient  $\max |\partial_z \tau(r=1)|$  (dark-colored line). The bulk surfactant concentration  $C_0$  is varied between  $10^{-5}$  and  $5 \times 10^{-4}$ , whereas the other simulation parameters are fixed:  $La = 100$ ,  $\beta = 0.7$ ,  $Sc = 10$ ,  $Sc_s = 100$ ,  $K_a = 10^4$ ,  $K_d = 10^2$ ,  $\chi = 0.01$ , and  $\varepsilon = 0.25$ .

small bulk surfactant concentrations, by multiplying  $C_0$  of a factor 5, i.e., increasing from  $C_0 = 10^{-5}$  to  $C_0 = 5 \times 10^{-5}$ , leads to a relative increment of  $t_c$  of about 10%. On the other hand, for the highest surfactant concentrations considered, increasing by a factor 5  $C_0$ , i.e., increasing from  $C_0 = 10^{-4}$  to  $C_0 = 5 \times 10^{-4}$ , almost doubles the closure time producing a relative increment of  $t_c$  of about 100%. This can be understood considering the nonlinear decrease of surface tension upon an increase of the interfacial surfactant concentration  $\Gamma$  for  $\Gamma \geq 1$  [see (3)].

The impact of the bulk surfactant concentration on the wall stresses is, however, less significant. Monitoring the tangential wall stress excursions,  $\Delta \tau_w(t) = \max_z \tau(r=1) - \min_z \tau(r=1)$ , Fig. 4 shows only minor changes of the stress peaks for  $C_0 \leq 10^{-4}$ , and increasing the bulk surfactant concentration to  $C_0 = 5 \times 10^{-4}$  decreases the tangential stress peak of about 20% with respect to  $C_0 = 10^{-4}$ . The quantitative characterizations of such a nonlinear process is affected by the model, hence they are accurate if a linear decrease of  $\sigma$  with  $\Gamma$  is dominant for  $\Gamma < 1$  and it asymptotically transitions to the Langmuir adsorption model [52] for  $\Gamma > 1$ . Quantitatively consistent observations are done for the maximum tangential stress gradients  $\max |\partial_z \tau_w|$ , while the peak normal wall stress excursions,  $\Delta p_w = \max_z p(r=1) - \min_z p(r=1)$ , are essentially not affected by  $C_0$  even for the highest bulk surfactant concentrations considered. A more remarkable impact is demonstrated in Fig. 4 for the maximum axial wall pressure gradient  $\max |\partial_z p_w|$ . This is in agreement with the observations of [8], who correlated the peak of  $\max |\partial_z p_w|$  to the capillary wave originated near the wall right after the bifrontal plug growth that enlarges the liquid plug. The net decrease of the local Laplace number due to the increase of surfactant concentration leads to weaker capillary stresses, hence to weaker  $\max |\partial_z p_w|$ .

The same qualitative impact on the airway closure process observed upon an increase of the initial bulk concentration  $C_0$  is also reproduced by an increase of the elasticity number  $\beta$ . This is demonstrated in Fig. 5 by varying  $\beta \in [0, 1.5]$  and fixing all the other model parameters to the

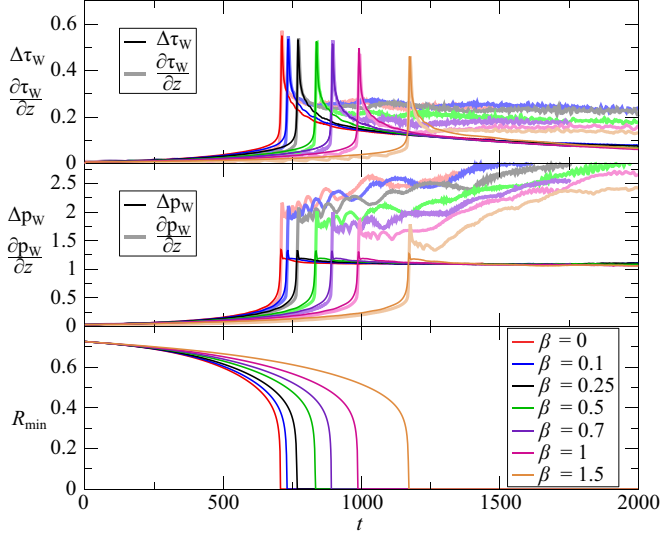


FIG. 5. Effect of the elasticity number, i.e., the strength of the surfactant. Bottom: minimum of the radial location of the interface,  $R_l$  (solid line). Middle: excursion of the normal stress distribution along the wall,  $\Delta p_w(t) = \max_z p(r=1) - \min_z p(r=1)$  (light-colored bold line), and the maximum axial pressure gradient  $\max |\partial_z p(r=1)|$  (dark-colored line). Top: excursion of the tangential stress distribution along the wall,  $\Delta \tau_w(t) = \max_z \tau(r=1) - \min_z \tau(r=1)$  (light-colored bold line), and the maximum axial wall shear stress gradient  $\max |\partial_z \tau(r=1)|$  (dark-colored line). The elasticity number  $\beta$  is varied between 0 and 1.5, whereas the other simulation parameters are fixed:  $C_0 = 10^{-4}$ ,  $La = 100$ ,  $Sc = 10$ ,  $Sc_s = 100$ ,  $K_a = 10^4$ ,  $K_d = 10^2$ ,  $\chi = 0.01$ , and  $\varepsilon = 0.25$ .

baseline values,  $C_0 = 10^{-4}$ ,  $La = 100$ ,  $Sc = 10$ ,  $Sc_s = 100$ ,  $K_a = 10^4$ ,  $K_d = 10^2$ ,  $\chi = 0.01$ , and  $\varepsilon = 0.25$ . In fact, increasing  $\beta$  enhances the impact of the interfacial surfactant concentration  $\Gamma$  on the surface tension [see (3)]. This leads to a reduction of the effective Laplace number that slows down the Plateau-Rayleigh instability and reduces the shear stress  $\Delta \tau_w$  and shear stress gradient  $\max |\partial_z \tau_w|$  at the wall. Moreover, increasing  $\beta$  is also impactful on the capillary wave propagating due to the bifrontal plug growth. As a result, the pressure gradient at the wall is tamed down by strong surfactants (high  $\beta$ ).

Beside the reduction of the effective Laplace number, an increase of  $\beta$  induces a variation of the Marangoni stresses. For  $\beta = 0$ , the surface tension is constant and the interfacial surfactant distribution does not induce any extra driving to the system. In this case, the surfactant plays the role of a passive tracer that can be absorbed and desorbed at the liquid-gas interface, but its concentration does not affect the liquid plug dynamics. For  $\beta \neq 0$ , the surfactant dynamics gets two-way coupled to the momentum equation via the interfacial gradient of surface tension. This leads to a rapid increase of the Marangoni stresses, well quantified by the Marangoni number  $Ma = -\partial_\Gamma \sigma RC_0 / \mu_L D_L$ . Such an increase saturates when the driving becomes too strong and concentrates the surfactant in a small portion of the interface, making  $-\partial_\Gamma \sigma$  pass from  $-\partial_\Gamma \sigma = \beta$  for  $\Gamma < 1$  to  $-\partial_\Gamma \sigma(\beta) = \beta \exp[\beta(1 - \Gamma)/(1 - \beta)]$  for  $\Gamma \geq 1$ . As observed by increasing  $C_0$ , the Marangoni driving represents an higher-order correction when compared to the reduction of the effective Laplace number.

### C. Effect of the adsorption $K_a$ and desorption $K_d$ coefficients, penetration depth $\chi$ , and Schmidt numbers $Sc$ and $Sc_s$

Except for  $\beta$  that directly act on  $\sigma$ , all the other nondimensional groups characterizing the physicochemical properties of the surfactant exert their impact on the liquid plug by affecting  $\Gamma$ .

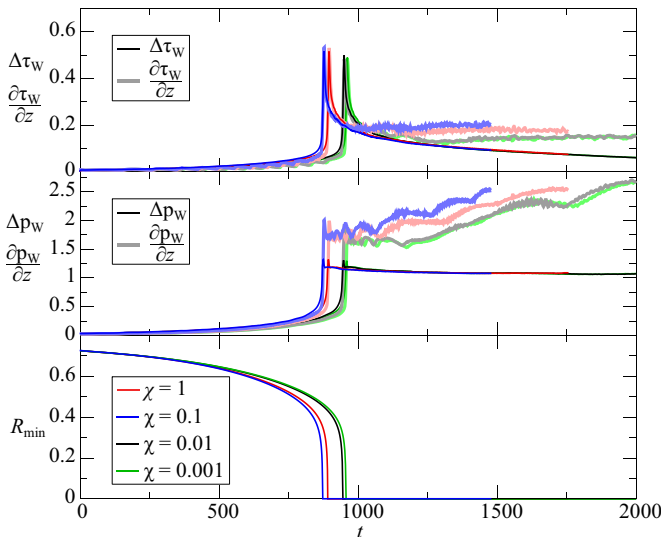


FIG. 6. Effect of the adsorption depth. Bottom: minimum of the radial location of the interface,  $R_l$  (solid line). Middle: excursion of the normal stress distribution along the wall,  $\Delta p_w(t) = \max_z p(r=1) - \min_z p(r=1)$  (light-colored bold line), and the maximum axial wall pressure gradient  $\max |\partial_z p(r=1)|$  (dark-colored line). Top: excursion of the tangential stress distribution along the wall,  $\Delta \tau_w(t) = \max_z \tau(r=1) - \min_z \tau(r=1)$  (light-colored bold line), and the maximum axial wall shear stress gradient  $\max |\partial_z \tau(r=1)|$  (dark-colored line). The penetration depth  $\chi$  is varied between 0.001 and 1, whereas the other simulation parameters are fixed:  $C_0 = 10^{-4}$ ,  $La = 100$ ,  $Sc = 10$ ,  $Sc_s = 100$ ,  $K_a = 10^4$ ,  $K_d = 10^2$ ,  $\beta = 0.7$ , and  $\varepsilon = 0.25$ .

This is the case of the adsorption  $K_a$  and desorption  $K_d$  coefficients, of the penetration depth  $\chi$ , and of the Schmidt numbers  $Sc$  and  $Sc_s$ .

Figure 6 demonstrates the minor impact of the penetration depth on the airway closure dynamics. The penetration depth is varied over three orders of magnitude,  $\chi \in [0.001, 1]$ , and the remaining parameters are set to the baseline values. Upon an increase of the penetration depth, Fig. 6 shows a speed-up of the airway closure (about 5% faster for  $\chi = 1$  than for  $\chi = 0.001$ ) and slightly increases the wall stress and stress gradients.

Similar observations can be extended to a variation of the adsorption and desorption coefficients, as well as to the Schmidt numbers. Decreasing ( $K_a$ ,  $K_d$ ) and ( $Sc$ ,  $Sc_s$ ) speeds up the airway closure, and has a negligible effect on the wall stresses. This is demonstrated in Figs. 7 and 8, where  $(K_a, K_d) \in ([10^3, 10^5], [10, 10^3])$  and  $(Sc, Sc_s) \in ([1, 10], [10, 100])$ , respectively. All the other parameters are set to the baseline values.

#### D. Effect of the Laplace number $La$

Another nondimensional group varied in our study is the Laplace number. The rationale of performing a dedicated parametric study is twofold: (1) we are interested in several bronchioles generations, whose Laplace number decays linearly with  $a$  and (2) we consider healthy and pathological cases, whose Laplace number can vary upon a change of  $\sigma_0$ . Three Laplace numbers are considered,  $La = 50, 100$ , and  $500$ . Moreover, in order to mimic the difference between a healthy patient and a surfactant deficient one, two values are assumed as reference for the initial surfactant concentration: (1) a clean case ( $C_0 = 0$ ), and (2) a surfactant contaminated case ( $C_0 = 10^{-4}$ ). All the combinations between the three Laplace numbers and the two initial concentrations are considered, for a total of six sets of parameters. All the other nondimensional groups are set according to the baseline case.

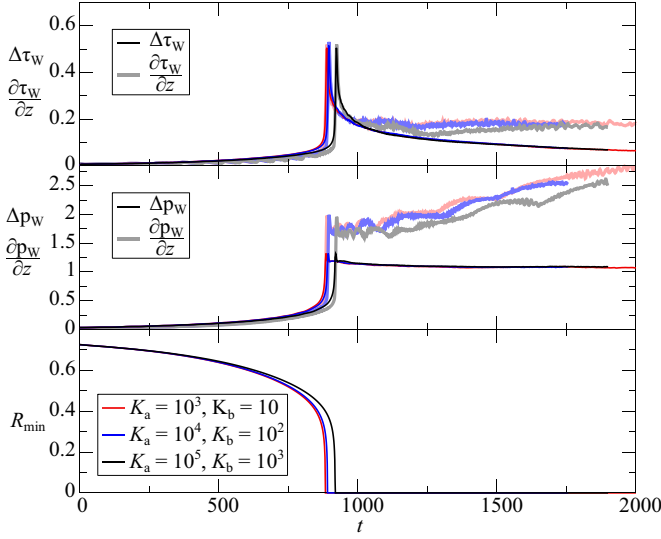


FIG. 7. Effect of the adsorption and desorption coefficients. Bottom: minimum of the radial location of the interface,  $R_I$  (solid line). Middle: excursion of the normal stress distribution along the wall,  $\Delta p_w(t) = \max_z p(r=1) - \min_z p(r=1)$  (light-colored bold line), and the maximum axial wall pressure gradient  $\max |\partial_z p(r=1)|$  (dark-colored line). Top: excursion of the tangential stress distribution along the wall,  $\Delta \tau_w(t) = \max_z \tau(r=1) - \min_z \tau(r=1)$  (light-colored bold line), and the maximum axial wall shear stress gradient  $\max |\partial_z \tau(r=1)|$  (dark-colored line). The adsorption and desorption coefficients,  $K_a$  and  $K_d$ , respectively, are varied between  $(K_a, K_d) \in ([10^3, 10^5], [10, 10^3])$ , whereas the other simulation parameters are fixed:  $C_0 = 10^{-4}$ ,  $La = 100$ ,  $Sc = 10$ ,  $Sc_s = 100$ ,  $\chi = 0.01$ ,  $\beta = 0.7$ , and  $\varepsilon = 0.25$ .

Figure 9 shows the effect of a change of  $La$  for clean and contaminated cases. In order to ease the comprehension of our numerical results in the context of physiologically relevant applications leading to an increase of surface tension, we plot the stresses and their axial gradient premultiplying them by  $La$ . This removes their dependence on  $\sigma_0$  coming from the capillary scaling; moreover, for the same reason, we divide the dimensionless time  $t$  by  $La$ . This demonstrates that an increase of surface tension leads to the well-expected acceleration of the Plateau-Rayleigh instability ( $\sigma_0 \uparrow$  implies  $La \sim \sigma_0 \uparrow$  that leads to  $\mu_L at_c / \sigma_0 \sim t_c / La \downarrow$ ), as well as to an increase of the wall stress and stress gradient ( $\sigma_0 \uparrow$  implies  $La \sim \sigma_0 \uparrow$  that leads, e.g., to  $\sigma_0 \Delta p_w / a \sim La \Delta p_w \uparrow$ ). We further stress that the increase of the stress level at epithelium due to surfactant deficiency can be as high as one order of magnitude (cf. data for  $La = 50$  and  $La = 500$  in the top and middle panels of Fig. 9). These same conclusions are well in agreement with the data of [8].

The net effect of the surfactant concentration  $C_0$  confirms the speeding up of the airway closure observed in Fig. 4 upon an increase of surfactant concentration. Figure 9 generalizes the validity of such a result over the whole range of interest of the Laplace numbers for healthy and pathological human bronchioles. Once again, we stress that increasing the surfactant concentration has a minor impact on the stresses and their gradient at the airway wall (cf. the clean and contaminated case in Fig. 9).

### E. Effect of the average nondimensional film thickness $\varepsilon$

The last parametric study we carry out involves the average nondimensional liquid film thickness  $\varepsilon$ . The physiological relevance of such a parameter is related to the pathologies inducing hypersecretion of mucus, hence enhancing  $\varepsilon$ .

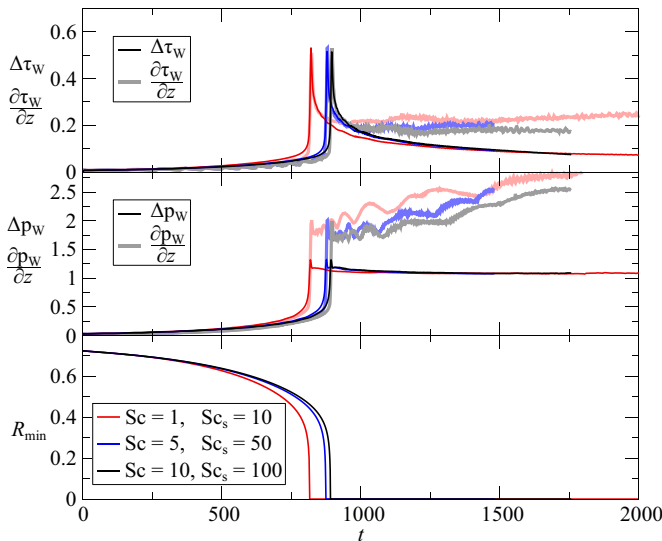


FIG. 8. Effect of the Schmidt numbers. Bottom: minimum of the radial location of the interface,  $R_l$  (solid line). Middle: excursion of the normal stress distribution along the wall,  $\Delta p_w(t) = \max_z p(r=1) - \min_z p(r=1)$  (light-colored bold line), and the maximum axial wall pressure gradient  $\max |\partial_z p(r=1)|$  (dark-colored line). Top: excursion of the tangential stress distribution along the wall,  $\Delta \tau_w(t) = \max_z \tau(r=1) - \min_z \tau(r=1)$  (light-colored bold line), and the maximum axial wall shear stress gradient  $\max |\partial_z \tau(r=1)|$  (dark-colored line). The bulk and interfacial Schmidt numbers,  $Sc$  and  $Sc_s$ , are varied between  $(Sc, Sc_s) \in ([1, 10], [10, 100])$ , whereas the other simulation parameters are fixed:  $C_0 = 10^{-4}$ ,  $La = 100$ ,  $K_a = 10^4$ ,  $K_d = 10^2$ ,  $\chi = 0.01$ ,  $\beta = 0.7$ , and  $\varepsilon = 0.25$ .

Figure 10 depicts the effect of the average film thickness on the airway closure, and it demonstrates that an increase of  $\varepsilon$  speeds up the Plateau-Rayleigh instability leading to airway closure on the wall stresses and tangential stress gradient. On the other hand, when considering the maximum normal stress gradient at the wall,  $\max |\partial_z p_w|$ , a remarkable increase is observed, especially for the postcoalescence phase. This is due to the origin of the pressure gradient peak, produced by the capillary wave advected near the wall by the bifrontal plug growth (see [8]). In fact, in agreement with the asymptotic theory for a Bretherton bubble [53], the gradient of the pressure scales inversely proportional to the average film thickness,  $\partial_z p_w \approx -\varepsilon \partial_z^3 \tilde{h}$ , where  $\tilde{h} = 1 - R_l$ .

### F. Stability diagram

Figure 11 reports an order-of-magnitude estimate of the inverse capillary time unit  $T^{-1} = \sigma_0 / \mu_L a$  for healthy and pathological cases of patients with large and small trachea. The gray markers denote the conditions for which gravitational effects cannot be neglected, hence our model does not strictly apply to them. Light-blue markers refer to the inverse airway capillary time unit of interest within our model framework. For pathological cases at the eighth and ninth generation the order of magnitude of  $T^{-1}$  is 500/s and 1000/s, respectively, whereas, including healthy cases for the 10th and 11th generation, the order of magnitude of the inverse capillary time unit increases to 2000/s and 5000/s, respectively, for healthy individuals and to 3000/s and 8500/s for pathological patients. Considering that for healthy patients the respiratory rate is about 20/min (one breath every 3 s [54]), the airway closure predicted in our model is considered physiologically relevant if it occurs before  $t \approx 3 \times 2000 = 6000$  capillary time units at the tenth generation, and  $t \approx 3 \times 5000 = 15000$  capillary time units at the 11th generation. The respiratory rate increases up to about 30/min for pathological conditions (one breath every 2 s [54]), hence the critical time



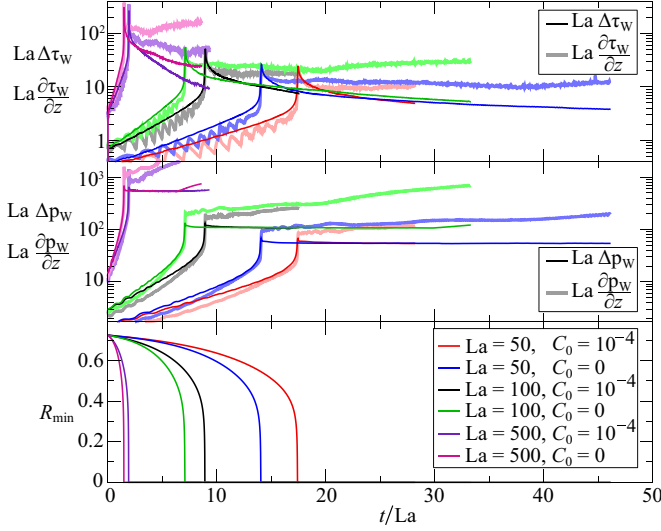


FIG. 9. Effect of the Laplace number. Bottom: minimum of the radial location of the interface,  $R_l$  (solid line). Middle: excursion of the normal stress distribution along the wall,  $\Delta p_w(t) = \max_z p(r=1) - \min_z p(r=1)$  (light-colored bold line), and the maximum axial wall pressure gradient  $|\partial_z p(r=1)|$  (dark-colored line). Top: excursion of the tangential stress distribution along the wall,  $\Delta \tau_w(t) = \max_z \tau(r=1) - \min_z \tau(r=1)$  (light-colored bold line), and the maximum axial wall shear stress gradient  $\max |\partial_z \tau(r=1)|$  (dark-colored line). The Laplace number and initial surfactant concentration,  $La$  and  $C_0$ , respectively, are varied between  $(La, C_0) \in \{[50, 500], \{0, 10^{-4}\}\}$  for a total of six cases, whereas the other simulation parameters are fixed:  $K_a = 10^4$ ,  $K_d = 10^2$ ,  $\chi = 0.01$ ,  $\beta = 0.7$ ,  $Sc = 10$ ,  $Sc_s = 100$ , and  $\varepsilon = 0.25$ .

threshold for pathological cases reduces to  $t \approx 2 \times 500 = 1000$  capillary time units at the eighth generation,  $t \approx 2 \times 1000 = 2000$  at the ninth generation, while it increases to  $t \approx 2 \times 3000 = 6000$  at the tenth generation, and  $t \approx 2 \times 8500 = 17000$  capillary time units at the 11th generation.

In the following, the stability diagram of our airway closure model will be discussed on the light of the previous considerations about the timescales of the corresponding biological system. We will denote as physiologically unstable all the conditions leading to the formation of a liquid plug within a breathing cycle. Whenever the liquid plug does not form (unconditional stability) or when it forms too late (conditional stability), we will assume that the airway closure would not occur in a corresponding physiological system, and we denote such cases as physiologically stable.

The stability threshold of the airway closure is evaluated for  $La = 100$ ,  $\beta = 0.7$ ,  $Sc = 10$ ,  $Sc_s = 100$ ,  $K_a = 10^4$ ,  $K_d = 10^2$ ,  $\chi = 0.01$ ,  $C_0 \in [0, 5 \times 10^{-4}]$ , and  $\varepsilon \in [0.125, 0.25]$ . Figure 12 shows the minimum radial coordinate of the liquid-gas interface as a function of time for the 25 parameter sets resulting from the combination between the five average film thicknesses  $\varepsilon$  (color coded from red to purple) and the five initial surfactant concentrations  $C_0$  (one per panel row). The figure is presented in three columns in order to highlight three very different timescales of interest: (1) for the first column  $t \in [0, 2000]$ , (2) for the second column  $t \in [0, 5000]$ , and (3) for the third column  $t \in [0, 30000]$ . On the abscissae, the critical closure times ( $t_c$ ) are indicated as a function of the physiological conditions ( $t_{cp}$  for pathological fast-breathing patients and  $t_{ch}$  for healthy patients with a regular breathing) and lung generation (e.g.,  $t_{cp8}$  denotes the critical closure time for the bronchioles of the eighth generation in a pathological patient). Such critical closure times correspond to the period of the breathing cycle (either 2 or 3 s for pathological  $t_{cp}T = 2$  s and healthy conditions  $t_{ch}T = 3$  s, respectively) nondimensionalized with respect to the bronchioles radius at the corresponding generation and they represent the longest time an airway closure can take in our model to qualify as physiologically admissible (physiologically unstable).

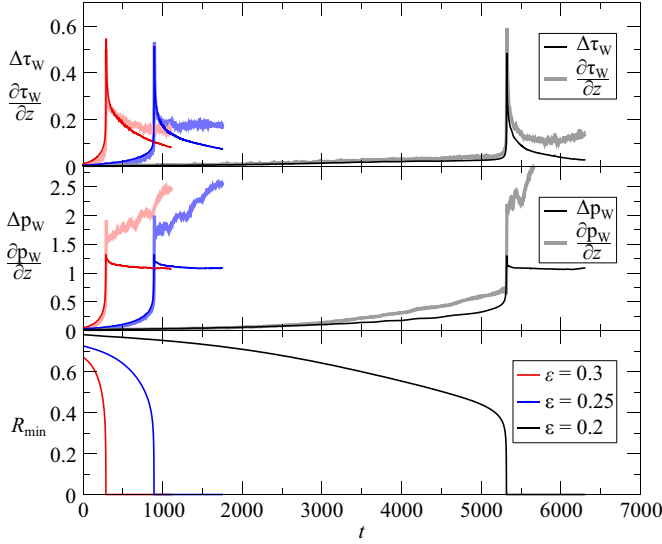


FIG. 10. Effect of initial liquid film thickness. Bottom: minimum of the radial location of the interface,  $R_l$  (solid line). Middle: excursion of the normal stress distribution along the wall,  $\Delta p_w(t) = \max_z p(r=1) - \min_z p(r=1)$  (light-colored bold line), and the maximum axial wall pressure gradient  $\max |\partial_z p(r=1)|$  (dark-colored line). Top: excursion of the tangential stress distribution along the wall,  $\Delta \tau_w(t) = \max_z \tau(r=1) - \min_z \tau(r=1)$  (light-colored bold line), and the maximum axial wall shear stress gradient  $\max |\partial_z \tau(r=1)|$  (dark-colored line). The average nondimensional film thickness  $\varepsilon$  is varied between 0.2 and 0.3, whereas the other simulation parameters are fixed:  $C_0 = 10^{-4}$ ,  $La = 100$ ,  $Sc = 10$ ,  $Sc_s = 100$ ,  $K_a = 10^4$ ,  $K_d = 10^2$ ,  $\beta = 0.7$ , and  $\chi = 0.01$ .

A summary of the physiological stability conditions is reported in the three diagrams depicted in Fig. 13 denoting with open markers the physiologically unstable configurations, while the full markers show the stable conditions. For fast-breathing pathological patients, the occlusion of distal airways can occur at generation 8 for a critical average thickness  $\varepsilon_c \in [0.2, 0.225]$  if  $C_0 \in [0, 10^{-4}]$

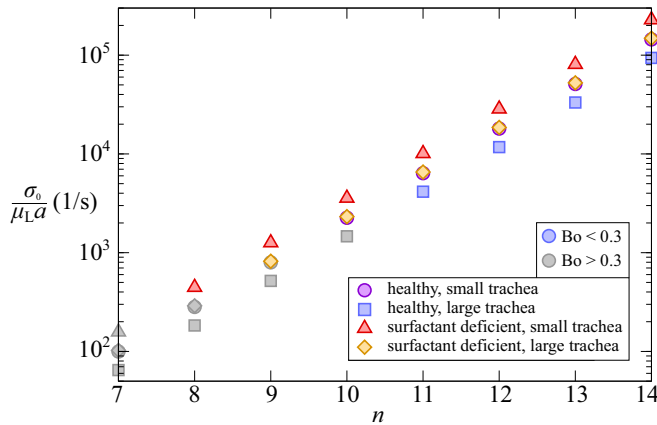


FIG. 11. Order-of-magnitude estimate of the inverse capillary time unit  $T^{-1} = \sigma_0 / \mu_L a$ . The light-blue markers denote the working framework of our investigation for which gravitational effects are safely neglected ( $Bo < 0.3$ ).

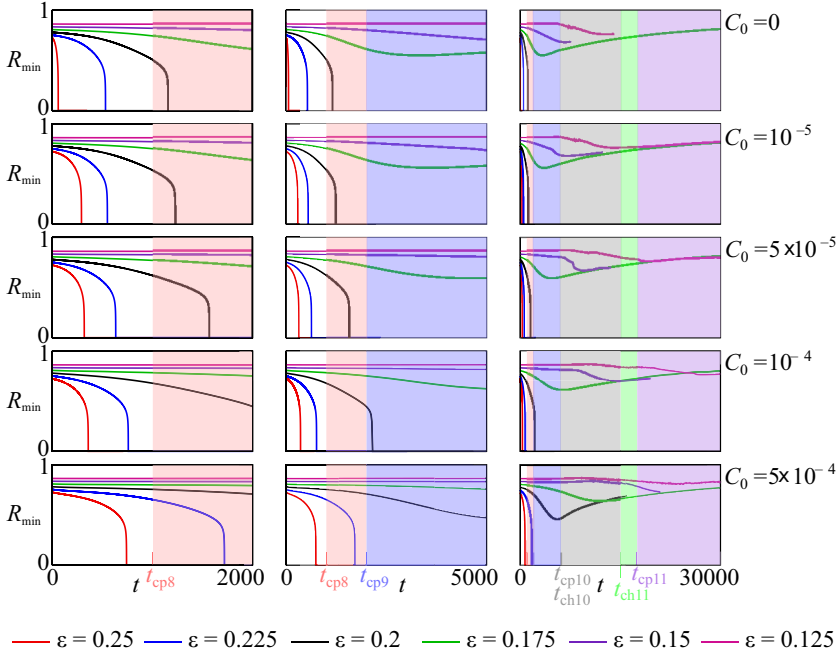


FIG. 12. Minimum of the radial location of the interface,  $R_l$ , color coded for five average film thicknesses ( $\varepsilon \in [0.125, 0.25]$ ) and arranged in rows, each of which corresponds to one of the five initial surfactant concentrations  $C_0 \in [0, 5 \times 10^{-4}]$ . All the other parameters are fixed:  $La = 100$ ,  $Sc = 10$ ,  $Sc_s = 100$ ,  $K_a = 10^4$ ,  $K_d = 10^2$ ,  $\beta = 0.7$ , and  $\chi = 0.01$ . Left, middle, and right panels denote the same airway closure dynamics over three relevant timescales:  $t \in [0, 2000]$  (left),  $t \in [0, 5000]$  (middle), and  $t \in [0, 30000]$  (right). The critical closure times  $t_c$  are shown on the abscissae for pathological  $t_{cp}T = 2s$  and healthy conditions  $t_{ch}T = 3s$ , normalized on the characteristic capillary unit time of a given generation (e.g.,  $t_{cp8}$  denotes the critical closure time at generation 8 for pathological fast-breathing patients).

[see Fig. 13(a)]. In such case, an increase of the initial surfactant concentration up to  $C_0 = 5 \times 10^{-4}$  induces an unconditionally stable condition that prevents airway closure from occurring for  $\varepsilon \in [0.2, 0.225]$  (see black line in Fig. 12) and shifts the critical condition to  $\varepsilon_c \in [0.225, 0.25]$ .

When considering ninth-generation bronchioles of fast-breathing pathological patients [see Fig. 13(b)], the physiologically critical average thickness reduces to  $\varepsilon_c \in [0.175, 0.2]$  if  $C_0 \in$

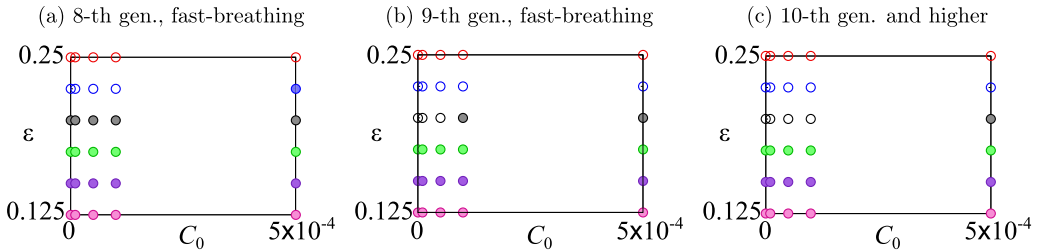


FIG. 13. Physiological stability diagram for bronchioles of the (a) eighth generation in fast-breathing pathological patients, (b) ninth generation in fast-breathing pathological patients, and (c) tenth and higher generations in all patients. Open markers denote physiologically unstable conditions, i.e., the airway closure occurs within a breathing cycle, while full markers depict physiologically stable cases.

$[0, 5 \times 10^{-5}]$  and  $\varepsilon_c \in [0.2, 0.225]$  if  $C_0 \in [10^{-5}, 5 \times 10^{-5}]$ . This decrease of stability of the system is well understood considering that the higher the generation, the smaller the bronchioles, and the more dominant the capillary forces become. Indeed, for distal airways the Plateau-Rayleigh instability at the origin of the airway closure leads more frequently to the occlusion of the airways when compared to lower-generation bronchioles. Such a stability loss is further confirmed by Fig. 13(c) where tenth and higher generations are considered. The critical average film thickness reduces to  $\varepsilon_c \in [0.175, 0.2]$  if  $C_0 \in [0, 10^{-4}]$  and  $\varepsilon_c \in [0.2, 0.225]$  if  $C_0$  is  $5 \times 10^{-5}$ .

We further stress that such critical values are significantly higher than the value predicted by [3],  $\varepsilon_c = 0.12$ . The reason is that the critical thickness computed in [3] reflects the onset of the Plateau-Rayleigh instability for thin films, which instability is indeed observed in our simulations (see initial decrease of  $R_{\min}$ ). However, the capillary instability gets further stabilized by the flow in the thick bulge and along the interface (see further increase of  $R_{\min}$  after an initial decrease for  $\varepsilon < 0.2$ ), which stabilization effect cannot be dealt with by employing lubrication theory.

## V. SUMMARY AND CONCLUSIONS

The effect of surfactant in human airway closure has been investigated by proposing a model for liquid plug formation in distal airways. We decided to simplify our mathematical model neglecting airway wall deformability, mobile ciliated surfaces and non-Newtonian effects. As a result, we focus on (1) the coupling between the bulk and interfacial surfactant dynamics (neglecting the surfactant micelles), (2) the Plateau-Rayleigh instability at the core of the airway closure, and (3) the bifrontal plug growth leading to a sudden postcoalescence increase of the stress level.

An extensive parametric study has been carried out by setting a baseline of reference for all the flow and surfactant parameters, and varying (almost always) one parameter at a time. The aim is to evaluate the stand-alone effect of each parameter.

At first, we varied the initial surfactant concentration showing that an increase of  $C_0$  can well have a remarkable impact on the Plateau-Rayleigh instability, postponing it significantly when increasing it from the clean case ( $C_0 = 0$ ) to the most contaminated case we consider ( $C_0 = 5 \times 10^{-4}$ ). Moreover, we observed a corresponding decrease of 20% of the tangential stress and stress gradient at the wall. Both such effects are also achieved by increasing the strength of the surfactant signified by the elasticity number  $\beta$  and they are both beneficial effects for the mechanics of a physiological airway closure. Therefore, our results show that the biological production of surfactant in human lungs does not have any negative mechanical effect as they help to prevent airway closure and, when it occurs, they limit the stress level on the epithelium.

The other nondimensional numbers characterizing the surfactant have little impact on the airway closure. In fact, varying over several orders of magnitude  $Sc$ ,  $Sc_s$ ,  $K_a$ ,  $K_d$ , and  $\chi$ , only minor effects on the main dynamics of the pre- and postcoalescence phases are observed. This highlights the general application of our results, as they are not very sensitive to the model parameters mimicking the surfactant dynamics in the bulk and at the interface. Moreover, our considerations also point towards good design rules for enhancing the performance of surfactant replacement therapies. In fact, rather than focusing on producing surfactant that dissolve faster/slower, penetrate deeper/shallower and adsorbe/desorbe more or less efficiently, from the sole mechanical point of view, a beneficial surfactant replacement therapy should aim for high  $\beta$  and large enough  $C_0$ . As also observed by other surfactant replacement mathematical models [55], too high surfactant concentrations are expected to saturate the benefit of corresponding surfactant replacement protocols.

Another parameter varied in our study is the Laplace number  $La$ . Upon an increase of the surface tension, the airway closure gets speed up with a consequent increase of the wall stress and stress gradient. It is remarkable that a surfactant deficiency brings the Laplace number from  $La = 50$  to  $La = 500$ , leading to a one-order-of-magnitude increase of the stress level at epithelium.

The last parameter we investigated is the average liquid film thickness  $\varepsilon$ . We show that airway closure with a thin liquid film is more dangerous because the pressure gradient produced by the corresponding postcoalescence capillary wave is larger. However, low  $\varepsilon$  significantly delays the

closure, hence tending to physiologically stabilize the process (in agreement with the experiments carried out by [19]). In this sense, airway closure with a thick film is expected to be much more frequent and probable than for thin liquid layers.

Finally, a dedicated two-parameter stability analysis in terms of  $\varepsilon$  and  $C_0$  has been carried out to investigate the effect of surfactant concentration for various liquid film thicknesses. Our results are produced for an initial perturbation of  $A = 10\%$ , and considering initial perturbations smaller than ours would lead to longer closure times. This calls for an adjustment of the physiological stability diagram in order to generalize our findings. Such a correction can be done by considering that the lubrication theory predicts a growth of the interfacial perturbation amplitude as  $A = A_0 e^{gt+ikz}$ , where  $A_0$  is the initial amplitude,  $k$  the wave number, and  $g = k^2(1 - k^2)/3$  [56]. The exponential growth predicted by the lubrication theory holds for infinitesimal amplitudes up to amplitudes larger than our  $A = 10\%$  [57]. Hence,  $A = A_0 e^{gt+ikz}$  can be used to calculate the time required by an arbitrary perturbation smaller than ours to lead to  $A = 10\%$ . The corresponding amplitude-growing time shall be added to our  $t_c$  for adjusting the physiological stability diagram whether an arbitrary perturbation smaller than 10% is considered. The conclusion of our physiological stability study points out that the increase of surfactant concentration shifts towards higher lung generations the occurrence of airway closure, in agreement with [10].

#### ACKNOWLEDGMENT

Support from National Institutes of Health (NIH), Grant No. R01-HL136141, and the Scientific and Technical Research Council of Turkey (TUBITAK), Grant No. 119M513, is kindly acknowledged.

- 
- [1] J. H. Widdicombe, S. J. Bastacky, D. X. Wu, and C. Y. Lee, Regulation of depth and composition of airway surface liquid, *Eur. Respir. J.* **10**, 2892 (1997).
  - [2] M. A. Sackner and C. S. Kim, Phasic flow mechanisms of mucus clearance, *Eur. J. Respir. Dis. Suppl.* **153**, 159 (1987).
  - [3] P. A. Gauglitz and C. J. Radke, An extended evolution equation for liquid film breakup in cylindrical capillaries, *Chem. Eng. Sci.* **43**, 1457 (1988).
  - [4] P. T. Macklem, D. F. Proctor, and J. C. Hogg, The stability of peripheral airways, *Respir. Physiol.* **8**, 191 (1970).
  - [5] I. A. Greaves, J. Hildebrandt, and J. F. G. Hoppin, in *Micromechanics of the Lung*, Comprehensive Physiology Vol. 3 (American Physiological Society, 2011), pp. 217–231.
  - [6] J. A. F. Plateau, *Statique expérimentale et théorique des liquides soumis aux seules forces moléculaires*, Vol. 2 (Gauthier-Villars, 1873).
  - [7] Lord Rayleigh, On the instability of cylindrical fluid surfaces, *London Edinburgh Dublin Philos. Mag. J. Sci.* **34**, 177 (1892).
  - [8] F. Romanò, H. Fujioka, M. Muradoglu, and J. B. Grothberg, Liquid plug formation in an airway closure model, *Phys. Rev. Fluids* **4**, 093103 (2019).
  - [9] D. Halpern and J. B. Grothberg, Fluid-elastic instabilities of liquid-lined flexible tubes, *J. Fluid Mech.* **244**, 615 (1992).
  - [10] D. Halpern and J. B. Grothberg, Surfactant effects on fluid-elastic instabilities of liquid-lined flexible tubes: A model of airway closure, *J. Biomech. Eng.* **115**, 271 (1993).
  - [11] D. Halpern, H. Fujioka, and J. B. Grothberg, The effect of viscoelasticity on the stability of a pulmonary airway liquid layer, *Phys. Fluids* **22**, 011901 (2010).
  - [12] O. Erken, F. Romanò, J. B. Grothberg, and M. Muradoglu, Capillary instability of a two-layer annular film: An airway closure model, *J. Fluid Mech.* **934**, A7 (2022).
  - [13] M. Heil, A. L. Hazel, and J. A. Smith, The mechanics of airway closure, *Resp. Physiol. Neurobiol.* **163**, 214 (2008).

- [14] C. F. Tai, S. Bian, D. Halpern, Y. Zheng, M. Filoche, and J. B. Grotberg, Numerical study of flow fields in an airway closure model, *J. Fluid Mech.* **677**, 483 (2011).
- [15] D. Huh III, H. Fujioka, Y. C. Tung, N. Futai, R. Paine, J. B. Grotberg, and S. Takayama, Acoustically detectable cellular-level lung injury induced by fluid mechanical stresses in microfluidic airway systems, *Proc. Natl. Acad. Sci. USA* **104**, 18886 (2007).
- [16] A. M. Bilek, K. C. Dee, and D. P. Gaver, Mechanisms of surface-tension-induced epithelial cell damage in a model of pulmonary airway reopening, *J. Appl. Physiol.* **94**, 770 (2003).
- [17] S. S. Kay, A. M. Bilek, K. C. Dee, and D. P. Gaver, Pressure gradient, not exposure duration, determines the extent of epithelial cell damage in a model of pulmonary airway reopening, *J. Appl. Physiol.* **97**, 269 (2004).
- [18] S. Bian, C. F. Tai, D. Halpern, Y. Zheng, and J. B. Grotberg, Experimental study of flow fields in an airway closure model, *J. Fluid Mech.* **647**, 391 (2010).
- [19] K. J. Cassidy, D. Halpern, B. G. Ressler, and J. B. Grotberg, Surfactant effects in model airway closure experiments, *J. Appl. Physiol.* **87**, 415 (1999).
- [20] F. Romanò, M. Muradoglu, H. Fujioka, and J. B. Grotberg, The effect of viscoelasticity in an airway closure model, *J. Fluid Mech.* **913**, A31 (2021).
- [21] M. Muradoglu, F. Romanò, H. Fujioka, and J. B. Grotberg, Effects of surfactant on propagation and rupture of a liquid plug in a tube, *J. Fluid Mech.* **872**, 407 (2019).
- [22] S. N. Ghadiali and D. P. Gaver, Biomechanics of liquid-epithelium interactions in pulmonary airways, *Resp. Physiol. Neurobi.* **163**, 232 (2008).
- [23] Y. Hu, F. Romanò, and J. B. Grotberg, Effects of surface tension and yield stress on mucus plug rupture: A numerical study, *J. Biomech. Eng.* **142**, 061007 (2020).
- [24] S. A. Bahrani, S. Hamidouche, M. Moazzen, K. Seck, C. Duc, M. Muradoglu, J. B. Grotberg, and F. Romanò, Propagation and rupture of elastoviscoplastic liquid plugs in airway reopening model, *J. Non-Newtonian Fluid Mech.* **300**, 104718 (2022).
- [25] Y. Zheng, H. Fujioka, S. Bian, Y. Torisawa, D. Huh, S. Takayama, and J. B. Grotberg, Liquid plug propagation in flexible microchannels: A small airway model, *Phys. Fluids* **21**, 071903 (2009).
- [26] J. B. Grotberg, Pulmonary flow and transport phenomena, *Annu. Rev. Fluid Mech.* **26**, 529 (1994).
- [27] J. B. Grotberg, Respiratory fluid mechanics and transport processes, *Annu. Rev. Biomed. Eng.* **3**, 421 (2001).
- [28] J. B. Grotberg and O. E. Jensen, Biofluid mechanics in flexible tubes, *Annu. Rev. Fluid Mech.* **36**, 121 (2004).
- [29] J. B. Grotberg, *Biofluid Mechanics: Analysis and Applications* (Cambridge University Press, Cambridge, UK, 2021).
- [30] G. Tryggvason, R. Scardovelli, and S. Zaleski, *Direct Numerical Simulations of Gas-Liquid Multiphase Flows* (Cambridge University Press, Cambridge, UK, 2011).
- [31] H. Fujioka and J. B. Grotberg, The steady propagation of a surfactant-laden liquid plug in a two-dimensional channel, *Phys. Fluids* **17**, 082102 (2005).
- [32] Y. Zheng, H. Fujioka, and J. B. Grotberg, Effects of gravity, inertia, and surfactant on steady plug propagation in a two-dimensional channel, *Phys. Fluids* **19**, 082107 (2007).
- [33] H. Fujioka III, D. Halpern, and D. P. Gaver III, A model of surfactant-induced surface tension effects on the parenchymal tethering of pulmonary airways, *J. Biomech.* **46**, 319 (2013).
- [34] H. A. Stone, A simple derivation of the time-dependent convective-diffusion equation for surfactant transport along a deforming interface, *Phys. Fluids* **2**, 111 (1990).
- [35] M. Muradoglu and G. Tryggvason, A front-tracking method for computation of interfacial flows with soluble surfactants, *J. Comput. Phys.* **227**, 2238 (2008).
- [36] M. Muradoglu and G. Tryggvason, Simulations of soluble surfactants in 3D multiphase flow, *J. Comput. Phys.* **274**, 737 (2014).
- [37] F. H. Harlow and J. E. Welch, Numerical calculation of time-dependent viscous incompressible flow of fluid with free surface, *Phys. Fluids* **8**, 2182 (1965).
- [38] S. O. Unverdi and G. Tryggvason, A front-tracking method for viscous incompressible multiphase flows, *J. Comput. Phys.* **100**, 25 (1992).



- [39] R. Borges, M. Carmona, B. Costa, and W. S. Don, An improved weighted essentially non-oscillatory scheme for hyperbolic conservation laws, *J. Comput. Phys.* **227**(6), 3191 (2008).
- [40] U. Olgac, A. D. Kayaalp, and M. Muradoglu, Buoyancy-driven motion and breakup of viscous drops in constricted capillaries, *Int. J. Multiphase Flow* **32**, 1055 (2006).
- [41] G. Tryggvason, B. Bunner, A. Esmaeeli, D. Juric, N. Al-Rawahi, W. Tauber, J. Han, S. Nas, and Y.-J. Jan, A front-tracking method for the computations of multiphase flow, *J. Comput. Phys.* **169**, 708 (2001).
- [42] C. Peskin, Numerical analysis of blood flow in the heart, *J. Comput. Phys.* **25**, 220 (1977).
- [43] E. R. Weibel, *Morphometry of the Human Lung*, Vol. 1 (Springer, Berlin, 1963).
- [44] R. G. Crystal, *The Lung: Scientific Foundations* (Lippincott-Raven, Lippincott, 1997).
- [45] J. A. Clements, E. S. Brown, and R. P. Johnson, Pulmonary surface tension and the mucus lining of the lungs: Some theoretical considerations, *J. Appl. Physiol.* **12**, 262 (1958).
- [46] J. H. Widdicombe, Regulation of the depth and composition of airway surface liquid, *J. Anat.* **201**, 313 (2002).
- [47] J. R. Lister, J. M. Rallison, A. A. King, L. J. Cummings, and O. E. Jensen, Capillary drainage of an annular film: The dynamics of collars and lobes, *J. Fluid Mech.* **552**, 311 (2006).
- [48] D. R. Otis, E. P. Ingenito, R. D. Kamm, and M. Johnson, Dynamic surface tension of surfactant TA: Experiments and theory, *J. Appl. Physiol.* **77**, 2681 (1994).
- [49] M. A. Launois-Surpas, T. Ivanova, I. Panaiotov, J. E. Proust, F. Puisieux, and G. Georgiev, Behavior of pure and mixed DPPC liposomes spread or adsorbed at the air-water-interface, *Colloid Polym. Sci.* **270**, 901 (1992).
- [50] M. L. Agrawal and R. D. Neuman, Surface diffusion in monomolecular films, II. Experiment and theory, *J. Colloid Interface Sci.* **121**, 366 (1988).
- [51] S. Schurch, H. Bachofen, J. Goerke, and F. Possmayer, A captive bubble method reproduces the in situ behavior of lung surfactant monolayers, *J. Appl. Physiol.* **67**, 2389 (1989).
- [52] V. G. Levich, *Physicochemical Hydrodynamics* (Prentice Hall, Englewood Cliffs, NJ, 1962).
- [53] F. P. Bretherton, The motion of long bubbles in tubes, *J. Fluid Mech.* **10**, 166 (1961).
- [54] M. A. Cretikos, R. Bellomo, K. Hillman, J. Chen, S. Finfer, and A. Flabouris, Respiratory rate: The neglected vital sign, *Med. J. Australia* **188**, 657 (2008).
- [55] M. Filoche, C.-F. Tai, and J. B. Grotberg, Three-dimensional model of surfactant replacement therapy, *Proc. Natl. Acad. Sci. USA* **112**, 9287 (2015).
- [56] P. S. Hammond, Nonlinear adjustment of a thin annular film of viscous fluid surrounding a thread of another within a circular pipe, *J. Fluid Mech.* **137**, 363 (1983).
- [57] D. Halpern and J. B. Grotberg, Nonlinear saturation of the Rayleigh instability due to oscillatory flow in a liquid-lined tube, *J. Fluid Mech.* **492**, 251 (2003).